

Search for the production of dark gauge bosons in the framework of Einstein-Cartan portal in the simulation of proton-proton collisions at $\sqrt{s} = 13.6$ TeV

S. Elgammal

Centre for Theoretical Physics, The British University in Egypt, P.O. Box 43, El Sherouk City, Cairo 11837, Egypt.

E-mail: sherif.elgammal@bue.edu.eg

ABSTRACT: In the present work, we study the possible production of the heavy neutral dark gauge boson (A') candidates, which originated from a simplified model based on the Einstein-Cartan gravity, in association with dark matter. This study has been performed by studying events with dimuon plus missing transverse energy produced in the simulated proton-proton collisions at the Large Hadron Collider, at 13.6 TeV center of mass energy and integrated luminosity of 52 fb^{-1} corresponding to the LHC run 3 circumstances during 2022 and 2023. We provide upper limits, in case no new physics has been discovered, on the masses of various particles in the model as, spin-1 (A'), as well as the heavy mediator (torsion field).

ARXIV EPRINT: [arXiv:2309.09184](https://arxiv.org/abs/2309.09184)

Contents

| | | |
|----------|---|-----------|
| 1 | Introduction | 1 |
| 2 | The simplified model in the framework of Einstein-Cartan gravity | 3 |
| 3 | Simulation of signal samples and SM backgrounds | 5 |
| 4 | Event selection | 5 |
| 5 | Results | 8 |
| 6 | Angular distributions in the Collins-Soper frame | 12 |
| 7 | Summary | 15 |

1 Introduction

The Standard Model of particle physics SM has been tested for more than 40 years [1], and its predictions agree very well with all experimental observations. However, the SM is nowadays considered a low-energy manifestation of other theories realized at high energy, generically known as BSM (Beyond the Standard Model) theories [2]. One motivation for BSM physics is to have a unified theory for the electromagnetic, weak, and strong interactions, in a unique Grand Unified Theory (GUT) [3]. The Super-Symmetry (SUSY) attempts to also include gravitation lead to models with extra spatial dimensions. These BSM models typically predict the existence of new dark particles at the TeV scale and higher.

The existence of heavy neutral bosons (Z') is a feature of many extensions of the Standard Model. They arise in extended gauge theories, including grand unified theories (GUT) [4], and other models like left-right symmetric models (LRM) [5]. A specific case is the sequential standard model (SSM), in which the Z' boson has the same coupling as the SM Z boson [6]. Model of extra dimensions like Randall and Sundrum model (RS) [7] predicts the existence of heavy Kaluza-Klein gravitons. Searches for these heavy dark neutral gauge bosons have been performed at the CMS and ATLAS experiments, at the Large Hadron Collider (LHC), with no evidence of their existence using the full RUN II period of the LHC data taking [8, 9].

Another alternative for the Randall and Sundrum model could be achieved through the Einstein-Cartan portal [10–15]. At which gravity (represented by the torsion field) can couple to the SM particles in addition to dark sector fermions, it provides a mechanism for producing the dark sector particles. It allows a chance for probing dark gauge boson (A'), which corresponds to a $U(1)_D$ symmetry, at LHC [16]. In this theory, the torsion

mass is in the TeV-scale regime, so that the A' can be produced with the high boost and missing transverse energy (E_T^{miss}) from dark-sector fermions. The search for the A' could be achieved at the LHC via its decay to dilepton (i.e. $A' \rightarrow l^+l^-$) and large E_T^{miss} .

Many searches for DM have been performed by analyzing the data collected by the CMS experiment during RUN II. These searches rely on the production of a visible object "X", which recoils against the large missing transverse energy from the dark matter particles leaving a signature of $(X + E_T^{miss})$ in the detector [17]. The visible particle could be an SM particle like Z [18, 19], W bosons [20, 21] or jets [22, 23], photon [24, 25] or SM Higgs boson [26, 27].

The ATLAS and CMS collaborations have previously conducted searches for the massive extra neutral gauge boson Z' decaying to dileptons. These searches are based on the Grand Unified Theory (GUT) and Supersymmetry [3–6]. Despite extensive efforts using the LHC data from the full RUN II period, no evidence of the existence of Z' has been found [8, 9]. Results from the CMS collaboration have excluded the existence of Z' in the mass range between 0.6 and 5.15 TeV with 95% Confidence Level (CL), while the ATLAS experiment has excluded the mass range between 0.6 and 5.1 TeV.

The direct detection of dark matter in underground experiments [28–32] presents various constraints. The model suggests that the interaction between dark matter and electrons can effectively explore light-dark matter. Exclusion limits confidently eliminate the possibility of dark matter with masses exceeding 4 MeV [33].

Indirect detection searches for dark matter are currently fascinating. The annihilation of dark matter into leptons or hadrons in space can potentially produce a signal of thermal WIMPs. The most reliable constraints for GeV dark matter annihilation into various final states are provided by Fermi-Lat observations of dwarf spheroidal galaxies [34, 35], AMS-02 positron fluxes [36, 37], and CMB [38–40] limits. These results indicate that the WIMP dark matter mass window from 20 GeV up to the unitarity limit [41] of 100 TeV remains largely open [42, 43].

In this analysis, we present a search for dark neutral gauge bosons (A'), which originated in a simplified model in the Einstein-Cartan portal, at the LHC simulated proton-proton collisions with 13.6 TeV center of mass energy corresponding to the LHC run 3 circumstances [44]. The topology of the studied simulated events is dimuon, from the decay of A' , plus large missing transverse energy attributed to dark matter. The signal of the above process is very similar to that coming from the decay of charginos pair into the lepton pair plus MET carried out by ATLAS [45].

In the next section 2, we will delve into the theoretical formalism of the $U(1)_D$ simplified model, which is based on Einstein-Cartan gravity, and its free parameters. Following that, in section 3, we will outline the simulation techniques utilized for generating events for both the signal and SM background samples in the subsequent section. Then, we will explain the selection cuts and the analysis strategy in the section 4. The results obtained from the current analysis will be presented in the section 5. We will then describe the results based on the angular distribution ($\cos\theta_{CS}$) in the Collins-Soper frame to distinguish signal from SM background events in the subsequent section 6. Finally, we will discuss the summary in the last section 7.

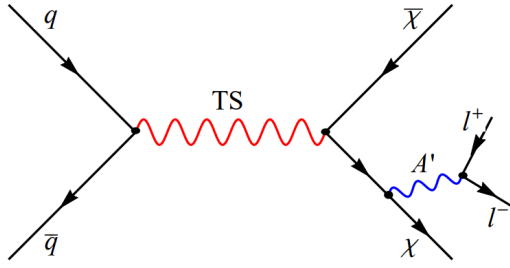


Figure 1: Feynman diagram for the simplified model based on Einstein-Cartan gravity; for the production of dark gauge boson (A') in association to dark matter (χ) pair [16].

2 The simplified model in the framework of Einstein-Cartan gravity

The analyzed simplified model is based on the Einstein-Cartan gravity, which has been discussed in [16], assumes the production of dark matters from proton-proton collisions at the LHC in addition to a new heavy neutral dark gauge boson A' .

The proposed dark gauge boson (A'_μ) can be produced through the process of pair annihilation of two quarks $q\bar{q}$ mediated by the heavy torsion field (S_ρ , which is the axial-vector part of the torsion tensor $T_{\mu\nu}^\lambda$ [16]), which then undergoes two dark matter particles (χ). Dark matter is heavy enough to decay to an A'_μ and another dark matter (χ) as shown in figure 1.

The interaction terms, in the effective Lagrangian, between the torsion field and Dirac fermion (ψ), is given by [16]

$$\bar{\psi}i\gamma^\mu(\partial_\mu + i\mathbf{g}_\eta\gamma^5 S_\mu + \dots)\psi.$$

According to the previous equation, the torsion field interacts with both the Standard Model (SM) and hidden fermions through its axial-vector part, with a universal coupling of $\mathbf{g}_\eta = 1/8$ at the classical level. This indicates that despite the SM and dark sectors existing in separate realms, the torsion field's universal coupling to any fermion is essential for generating dark-sector fermions. This occurs when SM fermions collide, leading to the subsequent radiation or decay of lighter dark-sector particles, producing dark gauge bosons with a significantly unsuppressed production cross-section. In the case of the dynamic torsion field, the classical value of $\mathbf{g}_\eta = 1/8$ becomes unstable due to quantum corrections, causing \mathbf{g}_η to vary with the energy scale [16]. Due to the torsion mass being in the TeV-scale regime, the A' is produced with the high boost and MET from dark-sector fermions is large where the SM backgrounds are low [16]. For this reason we have chosen $\mathbf{g}_\eta = 0.2$.

While the term in the effective Lagrangian at which the torsion field couples to the dark matter, and between dark gauge boson (A'_μ) and dark matter are given by [16]

$$\bar{\chi}(i\gamma^\mu D_\mu - M_\chi)\chi,$$

where $D_\mu = \partial_\mu + i\mathbf{g}_\eta\gamma^5 S_\mu + i\mathbf{g}_D A'_\mu$, M_χ is the dark matter mass and \mathbf{g}_D is the coupling of dark gauge boson to dark matter. The value of the coupling constant \mathbf{g}_D is taken from [16], which is $\mathbf{g}_D = 1.2$.

| Parameters | Description | optimized value |
|-------------------|---|-----------------------|
| \mathbf{g}_η | Coupling of torsion field to Dirac fermions | 0.2 [16] |
| \mathbf{g}_D | Coupling of dark gauge boson to dark matter | 1.2 [16] |
| M_χ | Mass of dark matter (χ) | 500 GeV [43, 46] |
| $M_{A'}$ | Mass of dark gauge boson (A') | [200, ..., 900] GeV |
| M_{ST} | Mass of torsion field (ST) | [1250, ..., 7000] GeV |
| Mass assumption | $M_{A'} < 2M_\chi$ [16] | |

Table 1: The simplified model parameters based on Einstein Cartan gravity and the chosen mass assumption [16].

| $M_{A'}$ \backslash M_{ST} | 1250 | 1500 | 1750 | 1800 | 1970 | 2000 | 3000 | 4000 | 5000 | 7000 |
|------------------------------|----------------------|-----------------------|------------------------|------------------------|------------------------|------------------------|-----------------------|-----------------------|----------------------|----------------------|
| 200 | 4.3×10^{-4} | 86.5×10^{-4} | 158.0×10^{-4} | 170.0×10^{-4} | 180.0×10^{-4} | 181.0×10^{-4} | 89.5×10^{-4} | 26.0×10^{-4} | 6.1×10^{-4} | 2.3×10^{-5} |
| 300 | 9.8×10^{-7} | 40.0×10^{-4} | 110.0×10^{-4} | 120.0×10^{-4} | 142.0×10^{-4} | 145.0×10^{-4} | 87.4×10^{-4} | 27.0×10^{-4} | 6.6×10^{-4} | 2.6×10^{-5} |
| 400 | 5.4×10^{-7} | 10.0×10^{-4} | 65.0×10^{-4} | 75.0×10^{-4} | 101.0×10^{-4} | 105.0×10^{-4} | 79.0×10^{-4} | 26.0×10^{-4} | 6.7×10^{-4} | 2.8×10^{-5} |
| 500 | 3.3×10^{-7} | 8.1×10^{-7} | 32.0×10^{-4} | 41.0×10^{-4} | 66.0×10^{-4} | 69.5×10^{-4} | 68.8×10^{-4} | 19.0×10^{-4} | 6.6×10^{-4} | 2.8×10^{-5} |
| 600 | 2.1×10^{-7} | 3.5×10^{-7} | 11.0×10^{-4} | 17.0×10^{-4} | 39.0×10^{-4} | 42.0×10^{-4} | 58.0×10^{-4} | 23.0×10^{-4} | 6.3×10^{-4} | 2.8×10^{-5} |
| 700 | 1.4×10^{-7} | 1.9×10^{-7} | 1.2×10^{-4} | 4.1×10^{-4} | 19.0×10^{-4} | 22.0×10^{-4} | 48.0×10^{-4} | 20.0×10^{-4} | 5.9×10^{-4} | 2.8×10^{-5} |
| 800 | 9.0×10^{-8} | 1.2×10^{-7} | 1.3×10^{-7} | 3.2×10^{-7} | 7.1×10^{-4} | 9.1×10^{-4} | 39.0×10^{-4} | 18.0×10^{-4} | 5.4×10^{-4} | 2.7×10^{-5} |
| 900 | 6.0×10^{-8} | 7.8×10^{-8} | 1.2×10^{-7} | 1.4×10^{-7} | 1.1×10^{-4} | 2.1×10^{-4} | 30.0×10^{-4} | 16.0×10^{-4} | 5.0×10^{-4} | 2.6×10^{-5} |

Table 2: The simplified model (based on Einstein Cartan gravity) cross-section measurements times branching ratios (in pb) calculated for different sets of the masses $M_{A'}$ (in GeV), and M_{ST} (in GeV), for the mass assumption given in table 1, with dark matter mass ($M_\chi = 500$ GeV), the following couplings constants $\mathbf{g}_\eta = 0.2$, $\mathbf{g}_D = 1.2$ and at $\sqrt{s} = 13.6$ TeV.

In general, the neutral dark gauge boson (A') subsequently decays to the SM fermion pairs [16]. In the current analysis, we choose the muonic decay of A' . According to [16], the highest significant branching ratio of $A' \rightarrow \mu^+ \mu^-$ could be reached if the following mass assumption listed in table 1 is satisfied,

In this model, there are several free parameters, including the mass of the torsion field (M_{ST}), the mass of the dark gauge boson ($M_{A'}$), the mass of the dark matter (M_χ), and the coupling constants (\mathbf{g}_η and \mathbf{g}_D). As mentioned earlier, the values of these coupling constants are set at $\mathbf{g}_\eta = 0.2$ and $\mathbf{g}_D = 1.2$. By using this combination of coupling values, we can achieve the highest possible cross-section times branching ratios. These model parameters are listed in table 1.

We are currently investigating the potential production of a heavy neutral dark gauge boson (A') at the LHC, with a mass ($M_{A'}$) that exceeds 100 GeV. According to the mass requirement specified in table 1, the dark matter mass needs to be substantial. Previous searches conducted in [43, 46] have indicated that there is a significant chance of detecting dark matter with masses between approximately 100 and 10000 GeV using various search techniques. As a result, we have designated the dark matter mass as $M_\chi = 500$ GeV.

The typical signature of this process consists of a pair of opposite sign muons from the decay of A' plus a large missing transverse energy due to the stable dark matter χ . The events we have studied are in the following topology: $\mu^+\mu^- + E_T^{miss}$. This is a clean channel for Standard Model (SM) backgrounds due to the optimization of the CMS detector for this decay channel. Additionally, according to reference [8], the fake rate of the QCD background was much smaller in the dimuon channels compared to the dielectron channel.

3 Simulation of signal samples and SM backgrounds

The SM background processes yielding muon pairs in the signal region are Drell-Yan ($DY \rightarrow \mu^+\mu^-$) and $DY \rightarrow \tau\tau$ productions, the production of top quark pairs ($t\bar{t} \rightarrow \mu^+\mu^- + 2b + 2\nu$), $tW \rightarrow \mu^+\mu^- + 2\nu + b$, and production of diboson ($W^+W^- \rightarrow \mu^+\mu^- + 2\nu$, $ZZ \rightarrow \mu^+\mu^- + 2\nu$ and $W^\pm Z \rightarrow \mu^\pm\mu^+\mu^- + \nu$). The second type of background is the jet background, which comes from the misidentification of jets as muons, where a jet or multijet passes the muons selection criteria. This kind of background originates from two processes: W+jets and QCD multijet. The contamination of single and multijet backgrounds in data is usually estimated from data using a so-called data-driven method which is explained in [8]. Nevertheless, they are irrelevant to our study because our analysis is based on MC simulations only, and no events from W+jets pass the analysis pre-selection presented in the following section.

The signal samples, for the simplified model (based on Einstein-Cartan gravity), and the corresponding SM processes have been generated using MadGraph5_aMC@NLO [47] interfaced to Pythia 8 for parton shower model and hadronization [48], and DELPHES [49] for a fast detector simulation of CMS experiment. They were generated from proton-proton collisions at the Large Hadron Collider at 13.6 TeV center of mass energy, which corresponds to the circumstances of run 3, with muon $p_T > 10$ GeV and $|\eta| < 3$ rad.

For the simplified model, with the use of mass assumption given in table 1, table 2 indicates the cross-section measurements times branching ratios calculated for different sets of the dark gauge boson (A') and torsion field (ST) masses. The simulated signals, used in this analysis, are private production samples, at which we used the matrix element event generator MadGraph5_aMC@NLO v2.6.7 [47].

All the Monte Carlo samples utilized in this analysis and their respective cross sections were computed in next-to-leading order and privately generated. Thus, the contributions of the signal samples and the SM background processes have been estimated from the Monte Carlo simulations, at which they are normalized to their corresponding cross-section and integrated luminosity of 52 fb^{-1} (the amount of certified data which is collected by CMS experiment so far during LHC run 3) [44].

4 Event selection

The selection of event, for the analysis, has been designed to reconstruct a final state with two high transverse momentum (p_T) muons in association with missing transverse energy accounting for the DM candidate. The selection is made using cuts applied on different kinematic parameters. Each of the two muons should pass the following pre-selection:

- p_T^μ (GeV) > 30,
- $|\eta^\mu|$ (rad) < 2.4,
- IsolationVarRhoCorr < 0.1,

IsolationVarRhoCorr represents the isolation cut in DELPHES software to reject muons produced inside jets. In this cut, it is required that the scalar p_T sum of all muon tracks within a cone of $\Delta R = 0.5$ around the muon candidate, excluding the muon candidate itself, should not exceed 10% of the p_T of the muon. This cut has been corrected for the pileup effect.

Thus, each event has been selected with two opposite charge muons, and the invariant mass of the dimuon is bigger than 60 GeV since we are looking for a resonance in the high mass regime.

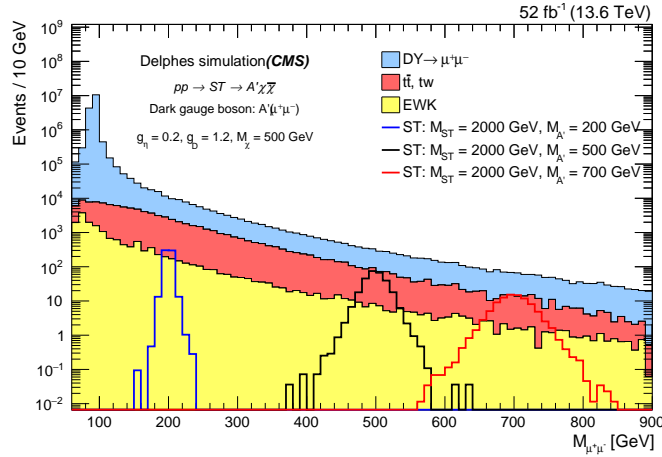


Figure 2: The measured dimuon invariant mass spectrum, for events passing selection 1 summarized in table 3, for the estimated SM backgrounds and different choices of dark gauge boson (A') masses generated based on the simplified model, with mass of torsion field ($M_{ST} = 2000$ GeV) and dark matter mass ($M_\chi = 500$ GeV).

Figure 2 shows the dimuon invariant mass distributions for events that meet the selection 1 criteria outlined in table 3. The cyan histogram depicts the $DY \rightarrow \mu^+\mu^-$ background, while the yellow histogram represents $DY \rightarrow \tau\tau$ and the backgrounds from vector boson pairs (WW , WZ , and ZZ). Additionally, the red histogram corresponds to the $t\bar{t}$ and tW backgrounds. These histograms are stacked. While the signals of the simplified model in the framework of Einstein-Cartan gravity, which have been generated with different masses of the neutral dark gauge boson A' with fixed values of the torsion field mass ($M_{ST} = 2000$ GeV) and dark matter mass ($M_\chi = 500$ GeV), are represented by different colored lines, and are overlaid.

The corresponding distribution of the missing transverse energy is depicted in figure 3, incorporating a single signal sample derived from the simplified model with a dark boson mass of $M_{A'} = 200$ GeV, a torsion field mass of $M_{ST} = 2000$ GeV, and a dark matter mass of $M_\chi = 500$ GeV. The Drell-Yan ($DY \rightarrow \mu^+\mu^-$) process primarily contributes to the low E_T^{miss} range. As this process does not produce undetectable particles, the measured E_T^{miss}

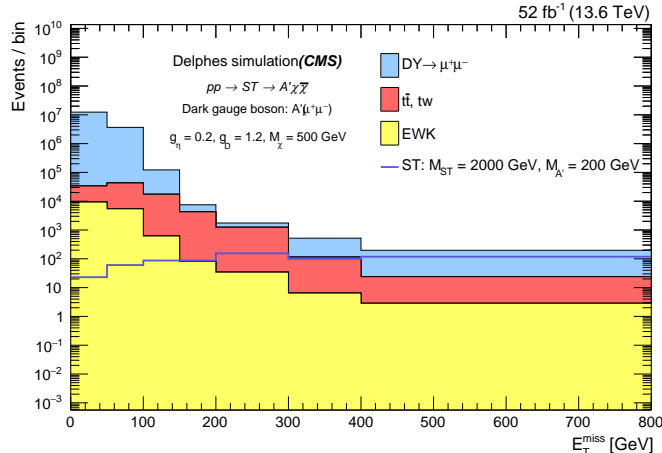


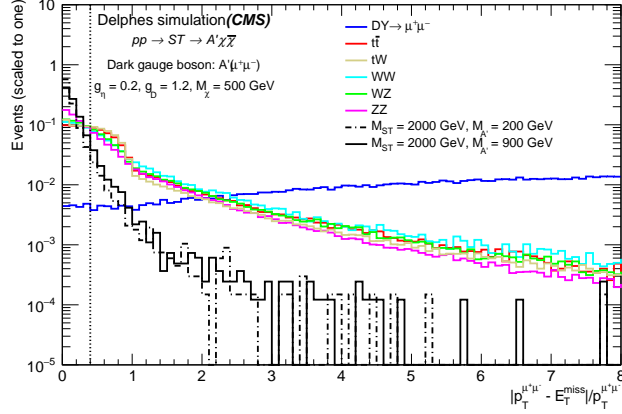
Figure 3: The distribution of the missing transverse energy, after selection 1; for the expected SM backgrounds, and mass of $A' = 200$ GeV produced by the simplified model, with the mass of torsion field ($M_{ST} = 2000$ GeV) and dark matter mass ($M_\chi = 500$ GeV).

results from limited detector acceptance and mismeasurement. It is evident from these figures that the background overwhelms the signal samples. Therefore, it is essential to implement stricter cut criteria to distinguish signals from SM backgrounds, as elaborated in the following paragraph.

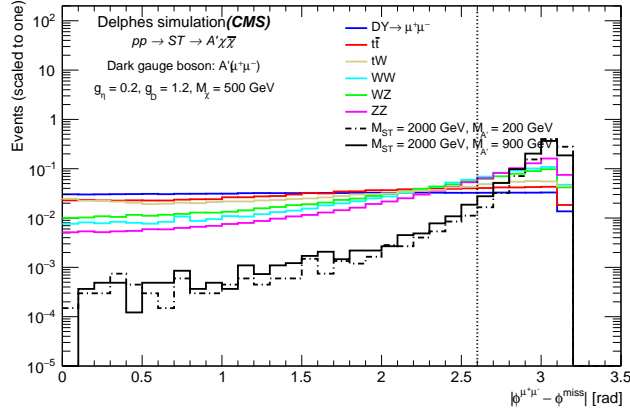
In addition to selection 1, extra tighter cuts have been designed to reduce the SM background further. These tight cuts are based on three variables: the first variable is related to the invariant mass of the dimuon, at which we restricted the invariant mass of the dimuon to a small range around the mass of the dark gauge boson A' to suppress backgrounds that do not peak at the A' mass, a requirement that $0.9 \times M_{A'} < M_{\mu^+\mu^-} < M_{A'} + 25$ as suggested in [16]. The second is the relative difference between the transverse momentum of dimuon ($p_T^{\mu^+\mu^-}$) and the missing transverse energy (E_T^{miss}), it has been selected to be less than 0.4. (i.e. $|p_T^{\mu^+\mu^-} - E_T^{\text{miss}}|/p_T^{\mu^+\mu^-} < 0.4$). The third one is $\Delta\phi_{\mu^+\mu^-, \vec{E}_T^{\text{miss}}}$, which is defined as difference in the azimuth angle between the dimuon direction and the missing transverse energy direction (i.e. $\Delta\phi_{\mu^+\mu^-, \vec{E}_T^{\text{miss}}} = |\phi^{\mu^+\mu^-} - \phi^{\text{miss}}|$), it has been selected to be greater than 2.6 rad.

For dimuon events passing selection 1, we present the distributions of two variables for the signal presentation of the simplified model corresponding to Einstein-Cartan gravity, along with SM backgrounds. The first variable is $|p_T^{\mu^+\mu^-} - E_T^{\text{miss}}|/p_T^{\mu^+\mu^-}$, shown in Figure 4(a), while the second variable is $\Delta\phi_{\mu^+\mu^-, \vec{E}_T^{\text{miss}}}$, shown in Figure 4(b). The model signals were generated with dark gauge boson mass $M_{A'} = 200$ and 900 GeV, torsion field mass $M_{ST} = 2000$ GeV, and dark matter mass $M_\chi = 500$ GeV. The distributions are scaled to one. The vertical dashed lines in both figures correspond to the chosen cut value per each variable.

These variables completely eliminate the $DY \rightarrow \tau\tau$ and ZZ backgrounds and significantly reduce the presence of $DY \rightarrow \mu^+\mu^-$, $t\bar{t}$, tW , WW , and WZ backgrounds. These adjustments are finely tuned to optimize the signal's sensitivity for various DM processes.



(a) $|p_T^{\mu^+\mu^-} - E_T^{miss}|/p_T^{\mu^+\mu^-}$



(b) $\Delta\phi_{\mu^+\mu^-}, \vec{E}_T^{miss}$

Figure 4: Distributions of $|p_T^{\mu^+\mu^-} - E_T^{miss}|/p_T^{\mu^+\mu^-}$ (a) and $\Delta\phi_{\mu^+\mu^-}, \vec{E}_T^{miss}$ (b) for two signals presentation of the simplified model corresponding to the Einstein-Cartan gravity with $M_{A'} = 200$ and 900 GeV and SM backgrounds, for dimuon events with each muon is passing the pre-selection cuts listed in table 3. The vertical dashed lines correspond to the chosen cut value per each variable. All histograms are normalized to unity to highlight qualitative features.

The dimuon invariant mass spectrum is shown in Figure 5 for events that meet the criteria listed in Table 3 (selection 2). The histograms represent the estimated SM backgrounds and various dark gauge boson (A') masses generated based on the simplified model, with a torsion field mass of $M_{ST} = 2000$ GeV and dark matter mass of $M_\chi = 500$ GeV.

5 Results

The shape-based analysis has been used based on the missing transverse energy distributions (E_T^{miss}), which are good discriminate variables since the signal distributions are

| Selection (1) | Selection (2) | Selection (3) |
|--|---|---|
| $p_T^\mu > 30 \text{ GeV}$ $ \eta^\mu < 2.4 \text{ rad}$ IsolationVarRhoCorr < 0.1 $M_{\mu^+\mu^-} > 60 \text{ GeV}$ | $p_T^\mu > 30 \text{ GeV}$ $ \eta^\mu < 2.4 \text{ rad}$ IsolationVarRhoCorr < 0.1 $M_{\mu^+\mu^-} > 60 \text{ GeV}$ $ p_T^{\mu^+\mu^-} - E_T^{\text{miss}} /p_T^{\mu^+\mu^-} < 0.4$ $\Delta\phi_{\mu^+\mu^-, \vec{E}_T^{\text{miss}}} > 2.6 \text{ rad}$ | $p_T^\mu > 30 \text{ GeV}$ $ \eta^\mu < 2.4 \text{ rad}$ IsolationVarRhoCorr < 0.1 $M_{\mu^+\mu^-} > 60 \text{ GeV}$ $ p_T^{\mu^+\mu^-} - E_T^{\text{miss}} /p_T^{\mu^+\mu^-} < 0.4$ $\Delta\phi_{\mu^+\mu^-, \vec{E}_T^{\text{miss}}} > 2.6 \text{ rad}$ $0.9 \times M_{A'} < M_{\mu^+\mu^-} < M_{A'} + 25$ |
| Pre-selection | Semi-final selection | Final selection |

Table 3: Summary of cut-based event selections used in the analysis.

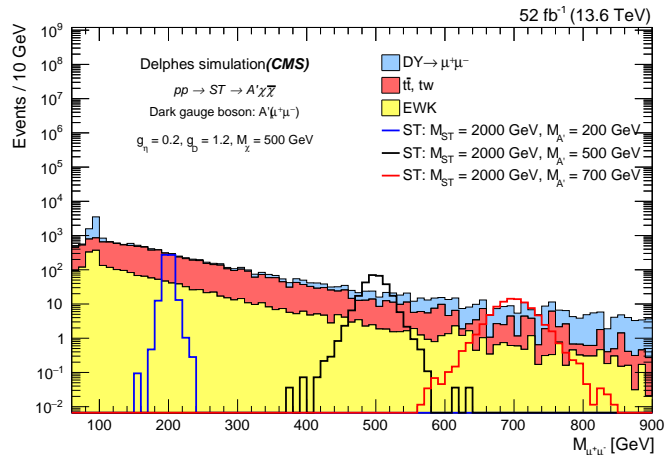


Figure 5: The dimuon invariant mass spectrum, for events passing selection 2 listed in table 3, for the estimated SM backgrounds and different choices of dark gauge boson (A') masses generated based on the simplified model, with mass of torsion field ($M_{ST} = 2000 \text{ GeV}$) and dark matter mass ($M_\chi = 500 \text{ GeV}$).

characterized by relatively large E_T^{miss} values compared to SM backgrounds. After applying selection 3 listed in table 3, the distribution of the missing transverse energy is illustrated in figure 6 for the expected SM backgrounds and one signal benchmark corresponding to the Einstein-Cartan gravity with $M_{A'} = 200 \text{ GeV}$ and $M_{ST} = 2000 \text{ GeV}$ is superimposed.

To calculate the significance of the signal, we used the Asimov formula given in [50],

$$S = \sqrt{2 \times \left((N_s + N_b) \log \left(1 + \frac{N_s}{N_b} \right) - N_s \right)}, \quad (5.1)$$

N_s and N_b represent the number of signals and the total number of SM background events that pass the selections (3) mentioned in tables 3.

In figure 7, the significance of A' discovery potential is plotted versus the integrated luminosity for the simplified model based on Einstein-Cartan gravity, with the dark matter mass fixed at $M_\chi = 500 \text{ GeV}$, $M_{ST} = 2000 \text{ GeV}$ and the coupling constants $g_\eta = 0.2$

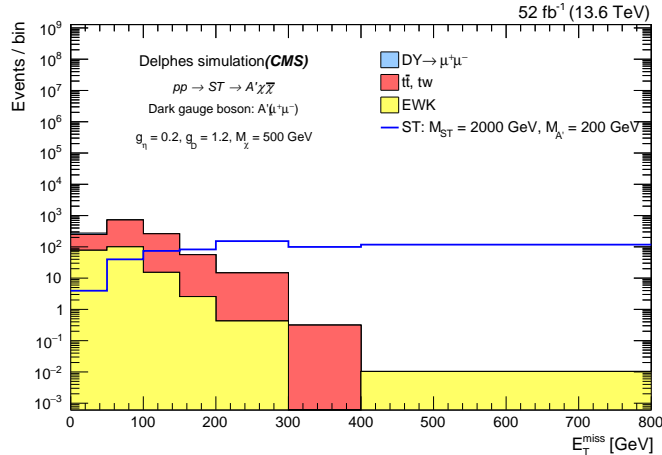


Figure 6: The distribution of the missing transverse energy, for events passing selection 3 presented in table 3, for the expected SM backgrounds and one signal benchmark corresponding to the Einstein-Cartan gravity with $M_{A'} = 200$ GeV is superimposed.

and $g_D = 1.2$. In the run3-LHC experiment, there is a possibility of detecting evidence for the torsion field with an integrated luminosity of more than 9 fb^{-1} for $M_{ST} = 2000$ GeV and $M_{A'} = 200$. Furthermore, for $M_{ST} = 2000$ GeV and $M_{A'} = 700$, a 5σ discovery can be achieved with an integrated luminosity exceeding 38 fb^{-1} , as illustrated in figure 7. However, according to the discovery potential based on the integrated luminosity, achieving a 5σ evidence is not feasible when the $M_{A'}$ masses exceed 700 GeV due to the significant decrease in the signal cross sections. To make a statistical interpretation for our results, we performed a statistical test based on the profile likelihood method, with the use of the modified frequentist construction CLs [51, 52] used in the asymptotic approximation [50] to derive exclusion limits on the product of signal cross sections and branching fraction $\text{Br}(A' \rightarrow \mu\mu)$ at 95% confidence level. The limits and significances presented have an adhoc flat 10% uncertainty systematic uncertainties taken into account to cover all possible systematic effects.

The 95% upper limit on the cross-section times the branching ratio versus the mass of torsion field M_{ST} , for the simplified model based on Einstein-Cartan gravity, is presented in figure 8, with the muonic decay of the A' and coupling constant values of $g_\eta = 0.2$ and $g_D = 1.2$ and dark matter mass $M_\chi = 500$ GeV. The black solid curve represents the simplified model for $M_{A'} = 200$ GeV. Based on figure 8, we exclude the torsion field (ST) production in the mass range between 1369 - 6241 GeV as shown from the expected median.

For the simplified model (based on Einstein-Cartan gravity), the cross-section times the branching ratio limit is presented in figure 9 as a function of the mediator's masses M_{ST} and the masses of the dark neutral gauge boson $M_{A'}$. The region between the respective pair of the expected 95% dotted line is excluded. The results from the inclusive signal regions exclude expected values of up to $1369 < M_{ST} < 6241$ GeV.

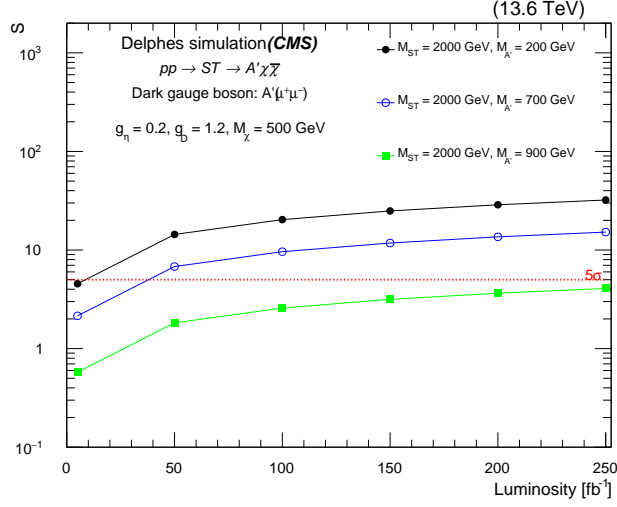


Figure 7: The significance was presented with the integrated luminosity for Einstein-Cartan gravity, considering different dark boson masses ($M_{A'}$). The values of the coupling constants were fixed at $g_\eta = 0.2$ and $g_D = 1.2$, with $M_{ST} = 2000$ GeV, and the dark matter mass set at $M_\chi = 500$ GeV. The red dotted line refers to the 5σ discovery potential.

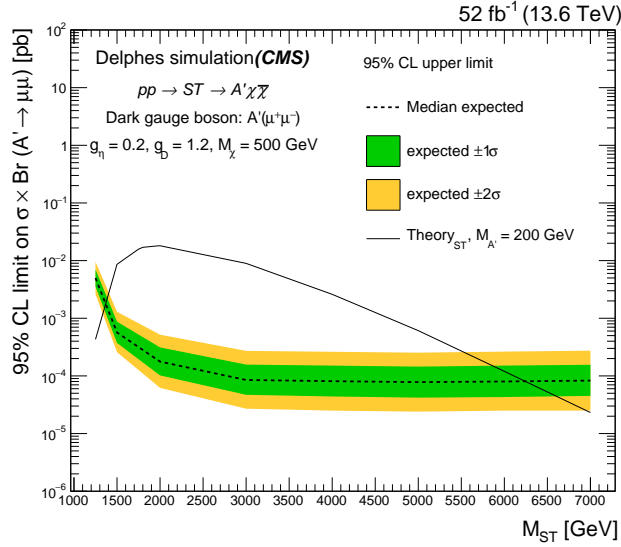


Figure 8: 95% CL upper limits on the cross-section times the branching ratio (expected), as a function of the mediator's mass (M_{ST}) based on Einstein-Cartan model, with the muonic decay of the A' . The black line represents the Einstein-Cartan gravity with $M_{A'} = 200$ GeV.

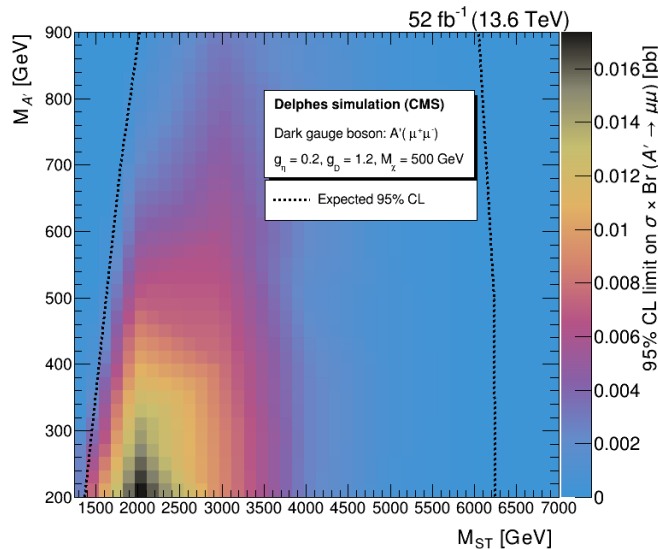


Figure 9: The 95% CL upper limits on the product of the cross-section and branching fraction from the inclusive search, for variations of pairs of the simplified model parameters (M_{ST} and $M_{A'}$). The filled region indicates the upper limit. The dotted black curve indicates the expected exclusions for the nominal A' cross-section.

6 Angular distributions in the Collins-Soper frame

In the Standard Model, the production of high-mass dimuon pairs is mainly controlled by the Drell-Yan process, which exhibits a significant forward-backward asymmetry [53, 54]. However, different scenarios beyond the Standard Model predict varied shapes for the $\cos\theta_{CS}$ distribution as defined in the Collins-Soper (SC) frame [55]. When there are more events than expected beyond the Standard Model, the angular distribution can be used to distinguish between these models.

When two partons collide, they can produce a pair of leptons known as l^+l^- . In our analysis, we study the angular distribution of the dimuon using the Collins-Soper frame, which minimizes the distortion of angular distributions caused by the transverse momenta of the incoming partons. This frame helps to minimize uncertainties caused by the unknown transverse momentum of the incoming quarks. To establish the orientation of the Collins-Soper frame, we use the longitudinal boost of the dilepton system. The angle $\cos\theta_{CS}$ can be calculated from quantities measured in the lab frame, as detailed in [56].

$$\cos\theta_{CS} = \frac{|Q_z|}{Q_z} \frac{2(P_1^+ P_2^- - P_1^- P_2^+)}{\sqrt{Q^2(Q^2 + Q_T^2)}}. \quad (6.1)$$

The symbols Q , Q_T , and Q_z represent the four-momentum, the transverse momentum, and the longitudinal momentum of the dimuon system, respectively. Similarly, P_1 (P_2) denotes the four-momentum of μ^- (μ^+), and E_i represents the energy of the muon. Additionally, P_i^\pm is defined as $(E_i \pm P_{z,i})/\sqrt{2}$. The graphs depicted in figure 10 show the distributions

| step | variable | requirements |
|---------------|---|--|
| Selection (4) | p_T^μ (GeV) | > 30 |
| | $ \eta^\mu $ (rad) | < 2.4 |
| | IsolationVarRhoCorr | < 0.1 |
| | $M_{\mu^+\mu^-}$ (GeV) | > 60 |
| | $ p_T^{\mu^+\mu^-} - E_T^{\text{miss}} /p_T^{\mu^+\mu^-}$ | < 0.4 |
| | $\Delta\phi_{\mu^+\mu^-, \vec{E}_T^{\text{miss}}}$ (rad) | > 2.6 |
| | Mass window (GeV) | $(0.9 \times M_{Z'}) < M_{\mu^+\mu^-} < (M_{Z'} + 25)$ |
| | E_T^{miss} (GeV) | > 200 |

Table 4: Summary of selection (4) for the angular distribution analysis.

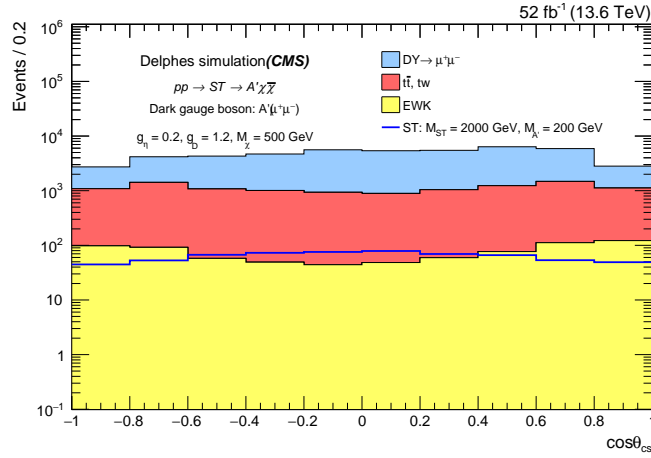
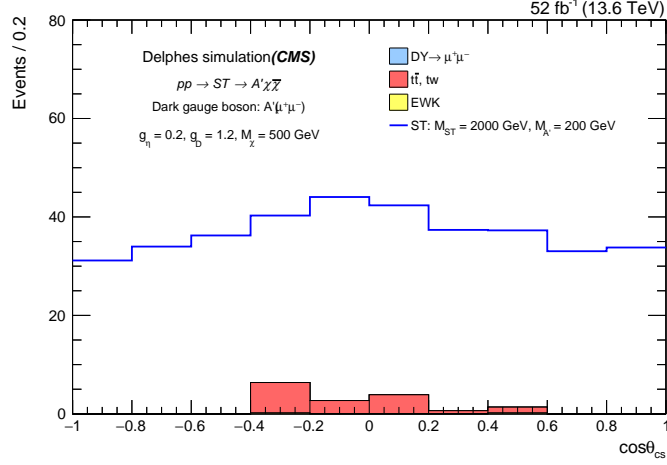


Figure 10: The distribution of $\cos\theta_{CS}$ in mass bin $180 < M_{\mu^+\mu^-} < 225$ GeV, for events passing pre-selection presented in table 3, for the expected SM backgrounds and one signal benchmark corresponding to the Einstein-Cartan gravity with $M_{A'} = 200$ GeV and $M_{ST} = 2000$ GeV is superimposed.

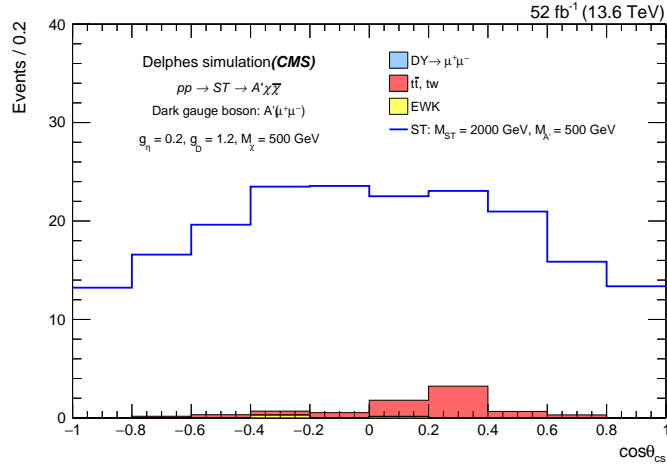
of the $\cos\theta_{CS}$ for dimuon events, in the mass bin $180 < M_{\mu^+\mu^-} < 225$ GeV, that have passed the pre-selection cuts listed in table 3 for one signal presentation of the simplified model corresponding to the Einstein-Cartan gravity with $M_{A'} = 200$ GeV, $M_{ST} = 2000$ GeV, and SM backgrounds.

In figure 11, the distributions of $\cos\theta_{CS}$ show the events that meet the newly optimized cuts for the Collins Soper analysis, as outlined in table 4. These events pertain to various presentations of the simplified model associated with Einstein-Cartan gravity, featuring $M_{ST} = 2000$ GeV and different $M_{A'}$ values: 200 GeV (a), 500 GeV (b), and 700 GeV (c), along with the standard model backgrounds.

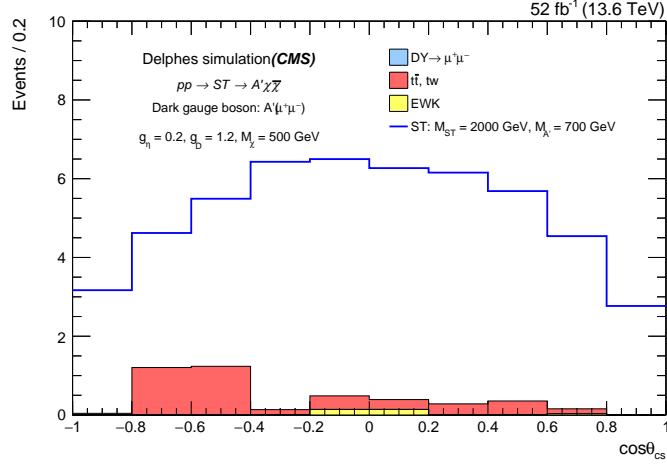
After implementing the cuts specified in table 4, it is evident that the signal sample can be easily distinguished from the SM backgrounds. The reductions in the DY, $t\bar{t}$, tW , and diboson backgrounds are substantial. Additionally, the potential contributions from the triboson and QCD multijet backgrounds, as discussed in [57], were found to be negligible



(a) $\cos\theta_{CS}$ distribution in mass bin $180 < M_{\mu^+\mu^-} < 225$ GeV



(b) $\cos\theta_{CS}$ distribution in mass bin $450 < M_{\mu^+\mu^-} < 525$ GeV



(c) $\cos\theta_{CS}$ distribution in mass bin $630 < M_{\mu^+\mu^-} < 725$ GeV

Figure 11: Distributions of $\cos\theta_{CS}$ for events passing the new cuts optimized for Collins Soper analysis and summarized in table 4 for several signals presentations of the simplified model corresponding to the Einstein-Cartan gravity with $M_{ST} = 2000$ GeV and different values of $M_{A'}$ = 200 GeV (a), 500 GeV (b), 700 GeV (c), and the SM backgrounds.

due to the stringent E_T^{miss} cut.

7 Summary

We have proposed a methodology to search for the dark neutral gauge bosons (A') at the LHC, which is produced in association with dark matter (χ) in the framework of $U(1)_D$ simplified model based on the Einstein-Cartan gravity. The presented analysis has been performed using the simulated proton-proton collisions corresponding to the LHC run 3 with 13.6 TeV center of mass energy, for an integrated luminosity of 52 fb^{-1} , which corresponds to the amount of certified data collected by CMS experiment so far during LHC run 3. Results from the muonic decay mode of A' are discussed, with fixing the values of the coupling constants to be $g_D = 1.2$, $g_\eta = 0.2$, and dark matter mass ($M_\chi = 500 \text{ GeV}$). We have considered the variations of several parameters of the signal model: the torsion field mass (M_{ST}) and the dark neutral gauge boson mass ($M_{A'}$).

The final analysis indicates that achieving a 5σ discovery of the A' dark gauge boson in the $\mu^+\mu^-$ decay channel is feasible. This can be accomplished for $M_{A'}$ values ranging from 200 to 700 GeV, given $M_{ST} = 2000 \text{ GeV}$, with an integrated luminosity of less than 40 fb^{-1} at the 13.6 TeV center of mass energy of the LHC run 3.

In addition, we have compared the anticipated distributions of the $\cos\theta_{CS}$ variable for high-mass Standard Model background events with that of a simplified model based on the Einstein-Cartan gravity. To improve distinguishing between signal events and SM backgrounds, we have applied powerful discrimination cuts that completely suppressed the $DY \rightarrow \mu^+\mu^-$, $DY \rightarrow \tau\tau$ and ZZ backgrounds.

In case no new physics has been discovered, the general version of the analysis, which uses only event-level kinematic variables, excludes models with $1369 < M_{ST} < 6241 \text{ GeV}$ at 95% confidence level (CL).

Acknowledgments

The author of this paper would like to thank Cao H. Nam, the author of [16], for his useful discussions about the theoretical models, and for sharing with us the Universal FeynRules Output (UFO) for the model that was used for the generation of the events. This paper is based on works supported by the Science, Technology, and Innovation Funding Authority (STDF) under grant number 48289.

Data Availability Statement: This manuscript has no associated data or the data will not be deposited.

References

- [1] F. Halzen and A. D. Martin, (1984), “Quarks And Leptons: An Introductory Course In Modern Particle Physics.” isbn: 0471887412, 9780471887416.
- [2] P. Langacker, “The standard model and beyond”, (2010). isbn: 9781420079067.
- [3] M. Cvetič and S. Godfrey, “Discovery and identification of extra gauge bosons”, arXiv:hep-ph/9504216.

- [4] A. Leike, “The Phenomenology of extra neutral gauge bosons”, *Phy. Rep.* 317, 143 (1999) [arXiv:hep-ph/9805494].
- [5] M. Cvetič, P. Langacker and B. Kayser, “Determination of g-R / g-L in left-right symmetric models at hadron colliders”, *Phys. Rev. Lett.* 68 (1992) 2871.
- [6] S. Dimopoulos and H. Georgi, “Softly Broken Supersymmetry And SU(5)”, *Nucl. Phys. B* 193 (1981) 150.
- [7] L. Randall and R. Sundrum, “A large mass hierarchy from a small extra dimension”, *Phys. Rev. Lett.* 83 (1999) 3370 [arXiv:hep-ph/9905221].
- [8] CMS Collaboration, Search for resonant and nonresonant new phenomena in high-mass dilepton final state at $\sqrt{s} = 13$ TeV, *JHEP* 07 (2021) 208 [arXiv:2103.02708v2] [hep-ex].
- [9] ATLAS Collaboration, Search for new non-resonant phenomena in high-mass dilepton final states with the ATLAS detector, *JHEP* 11 (2020) 05.
- [10] T.W. B. Kibble, Lorentz Invariance and the Gravitational Field. *Journal of Mathematical Physics.* 2 (2): 212–221 (1961).
- [11] Sciama, D. W., The Physical Structure of General Relativity. *Reviews of Modern Physics.* 36 (1): 463–469 (1964-01-01).
- [12] Hehl, Friedrich W.; von der Heyde, Paul; Kerlick, G. David; Nester, James M. General relativity with spin and torsion: Foundations and prospects. *Reviews of Modern Physics.* 48 (3): 393–416.
- [13] Dimitri Tsoubelis, Gravitational Field of a Spin-Polarized Cylinder in the Einstein-Cartan Theory of Gravitation. *Phys. Rev. Lett.* 51, 2235 (1983).
- [14] M. Shaposhnikov, A. Shkerin, I. Timiryasov, and S. Zell, Einstein-Cartan gravity, matter, and scale-invariant generalization, *J. High Energy Phys.* 10 (2020) 177.
- [15] M. Shaposhnikov, A. Shkerin, I. Timiryasov, and S. Zell, Einstein-Cartan Portal to Dark Matter. *Phys. Rev. Lett.* 126, 161301 (2021).
- [16] Cao H. Nam, Probing dark gauge boson via Einstein-Cartan portal. *Phys. Rev. D* 105, 075015 (2022) [arXiv:2112.10446] [hep-ph].
- [17] Krovi AniruDF, Low Ian and Zhang Yue, Broadening dark matter searches at the LHC: mono-X versus darkonium channels. *JHEP* 10 (2018) 026 [arXiv:1807.07972] [hep-ph].
- [18] CMS Collaboration, Search for dark matter produced in association with a leptonically decaying Z boson in proton-proton collisions at $\sqrt{s} = 13$ TeV. *Eur. Phys. J. C* 81 (2021) 13; Erratum: *Eur. Phys. J. C* 81 (2021) 333.
- [19] ATLAS Collaboration, Search for associated production of a Z boson with an invisibly decaying Higgs boson or dark matter candidates at $\sqrt{s} = 13$ TeV with the ATLAS detector. *Phys. Lett. B* 829 (2022) 137066.
- [20] ATLAS Collaboration, Search for dark matter produced in association with a single top quark and an energetic W boson in $\sqrt{s} = 13$ TeV pp collisions with the ATLAS detector. *Eur. Phys. J. C* 83 (2023) 603.
- [21] ATLAS Collaboration, Search for new particles in events with a hadronically decaying W or Z boson and large missing transverse momentum at $\sqrt{s} = 13$ TeV using the ATLAS detector. CERN-EP-2024-128, arXiv:2406.01272v1 [hep-ex].

- [22] ATLAS Collaboration, Search for new phenomena in events with an energetic jet and missing transverse momentum in pp collisions at $\sqrt{s} = 13$ TeV with the ATLAS detector. *Phys. Rev. D* 103 (2021) 112006.
- [23] CMS Collaboration, Search for new particles in events with energetic jets and large missing transverse momentum in proton-proton collisions at $\sqrt{s} = 13$ TeV. *JHEP* 11 (2021) 153.
- [24] CMS Collaboration, Search for new physics in the monophoton final state in proton-proton collisions at $\sqrt{s} = 13$ TeV, *JHEP*. 10 (2017) 073.
- [25] ATLAS collaboration, Search for dark matter at $\sqrt{s} = 13$ TeV in final states containing an energetic photon and large missing transverse momentum with the ATLAS detector, *Eur. Phys. J. C* 77 (2017) 393.
- [26] CMS Collaboration, Search for dark matter particles produced in association with a Higgs boson in proton-proton collisions at $\sqrt{s} = 13$ TeV, *JHEP* 03 (2020) 025, [arXiv:1908.01713v2] [hep-ex].
- [27] ATLAS Collaboration, Combination and summary of ATLAS dark matter searches interpreted in a 2HDM with a pseudo-scalar mediator using 139 fb^{-1} of $\sqrt{s} = 13$ TeV pp collision data. CERN-EP-2023-088, arXiv:2306.00641 [hep-ex].
- [28] J. Angle et al. (XENON10 Collaboration), Search for light dark matter in XENON10 data, *Phys. Rev. Lett.* 107, 051301 (2011); 110, 249901(E) (2013).
- [29] E. Aprile et al. (XENON100 Collaboration), Observation and applications of single-electron charge signals in the XENON100 experiment, *J. Phys. G* 41, 035201 (2014).
- [30] E. Aprile et al., Light dark matter search with ionization signals in XENON1T, *Phys. Rev. Lett.* 123, 251801 (2019).
- [31] L. Barak et al. (SENSEI Collaboration), SENSEI: Directdetection results on sub-GeV dark matter from a new skipper CCD, *Phys. Rev. Lett.* 125, 171802 (2020).
- [32] C. Cheng et al. (PandaX-II Collaboration), Search for light dark matter–electron scattering in the PandaX-II experiment, *Phys. Rev. Lett.* 126, 211803 (2021).
- [33] Louis Hamaide and Christopher McCabe, Fueling the search for light dark matter–electron scattering with spherical proportional counters, *Phys. Rev. D* 107, 063002.
- [34] M. Ackermann et al. (Fermi-LAT Collaboration), Searching for dark matter annihilation from Milky Way dwarf spheroidal galaxies with six years of fermi large area telescope data, *Phys. Rev. Lett.* 115, 231301 (2015).
- [35] A. Albert et al. (DES and Fermi-LAT Collaborations), Searching for dark matter annihilation in recently discovered milky way satellites with fermi-LAT, *Astrophys. J.* 834, 110 (2017).
- [36] M. Aguilar et al. (AMS Collaboration), Electron and positron fluxes in primary cosmic rays measured with the alpha magnetic spectrometer on the international space station, *Phys. Rev. Lett.* 113, 121102 (2014).
- [37] L. Accardo et al. (AMS Collaboration), High statistics measurement of the positron fraction in primary cosmic rays of 0.5–500 GeV with the alpha magnetic spectrometer on the international space station, *Phys. Rev. Lett.* 113, 121101 (2014).
- [38] P. A. R. Ade et al. (Planck Collaboration), Planck 2015 results - XIII. Cosmological parameters, *Astron. Astrophys.* 594, A13 (2016).

- [39] T. R. Slatyer, N. Padmanabhan, and D. P. Finkbeiner, CMB Constraints on WIMP Annihilation: Energy Absorption During the Recombination Epoch, *Phys. Rev. D* 80 (2009) 043526, [arXiv:0906.1197].
- [40] T. R. Slatyer, Indirect dark matter signatures in the cosmic dark ages. I. Generalizing the bound on s-wave dark matter annihilation from Planck results, *Phys. Rev. D* 93 (2016), no. 2 023527, [arXiv:1506.03811].
- [41] J. Smirnov and J. F. Beacom, TeV-Scale Thermal WIMPs: Unitarity and its Consequences, *Phys. Rev. D* 100 (2019), no. 4 043029, [arXiv:1904.11503].
- [42] G. Steigman, B. Dasgupta, and J. F. Beacom, Precise Relic WIMP Abundance and its Impact on Searches for Dark Matter Annihilation, *Phys. Rev. D* 86 (2012) 023506, [arXiv:1204.3622].
- [43] R. K. Leane, T. R. Slatyer, J. F. Beacom, and K. C. Ng, GeV-scale thermal WIMPs: Not even slightly ruled out, *Phys. Rev. D* 98 (2018), no. 2 023016, [arXiv:1805.10305].
- [44] <https://twiki.cern.ch/twiki/bin/view/CMSPublic/LumiPublicResults>.
- [45] ATLAS Collaboration, Search for electroweak production of charginos and sleptons decaying into final states with two leptons and missing transverse momentum in $\sqrt{s} = 13$ TeV pp collisions using the ATLAS detector, *Eur. Phys. J. C* (2020) 80:123.
- [46] Jan Conrad and Olaf Reimer, Indirect dark matter searches in Gamma- and Cosmic Rays, *Nature Physics*, Volume 13, Issue 3, pp. 224-231 (2017).
- [47] Johan Alwall, Michel Herquet, Fabio Maltoni, Olivier Mattelaer, and Tim Stelzer. *MadGraph 5 : Going Beyond*. *JHEP*, 06:128, 2011.
- [48] T. Sjöstrand, S. Ask, J.R. Christiansen, R. Corke, N. Desai, P. Ilten, S. Mrenna, S. Prestel, C.O. Rasmussen, P.Z. Skands. An Introduction to PYTHIA 8.2, *Comput. Phys. Commun.* 191 (2015) 159–177, arXiv:1410.3012 [hep-ph].
- [49] J. de Favereau, C. Delaere, P. Demin, A. Giammanco, V. Lemaître, A. Mertens, M. Selvaggi, DELPHES 3, A modular framework for fast simulation of a generic collider experiment, *JHEP* 1402 (2014).
- [50] G. Cowan et al., Asymptotic formulae for likelihood-based tests of new physics, *Eur. Phys. J. C* 71 (2011), p. 1554, doi: 10.1140/epjc/s10052-011-1554-0, arXiv: 1007.1727 [physics.data-an], Erratum: *Eur. Phys. J. C* 73 (2013) 2501.
- [51] A. L. Read, Presentation of search results: the CLs technique, *J. Phys. G: Nucl. Part.Phys.* 28 (2002) 2693, doi:10.1088/0954-3899/28/10/313.
- [52] T. Junk, Confidence level computation for combining searches with small statistics, *Nuclear Instruments and Methods in Physics Research Section A: Accelerators, Spectrometers, Detectors and Associated Equipment*, Volume 434, Issues 2–3, 1999, Pages 435-443, ISSN 0168-9002, [https://doi.org/10.1016/S0168-9002\(99\)00498-2](https://doi.org/10.1016/S0168-9002(99)00498-2).
- [53] ATLAS Collaboration, Measurement of the angular coefficients in Z-boson events using electron and muon pairs from data taken at $\sqrt{s} = 8$ TeV with the ATLAS detector. *JHEP* 08 (2016) 159.
- [54] CMS Collaboration, Measurement of the Drell-Yan forward-backward asymmetry at high dilepton masses in proton-proton collisions at $\sqrt{s} = 13$ TeV. *JHEP* 08 (2022) 063.

- [55] J. Collins and D. Soper, Angular distribution of dileptons in high-energy hadron collisions. *Phys. Rev. D.*, 16(7):2219–2225, 1977.
- [56] CMS Collaboration, Forward-backward asymmetry of Drell-Yan lepton pairs in pp collisions at $\sqrt{s} = 8$ TeV. *Eur. Phys. J. C* 76 (2016) 325.
- [57] Akanksha Bhardwaj, Juhi Dutta, Partha Konar, Biswarup Mukhopadhyayad and Santosh Kumar Raie, Boosted jet techniques for a supersymmetric scenario with gravitino LSP. *JHEP*10 (2020) 083.